Received: 6 December 2023 | Accepted: 23 May 2024

DOI: 10.1111/2041-210X.14365

Methods in Ecology and Evolution

RESEARCH ARTICLE

Macrophenological dynamics from citizen science plant occurrence data

Karin Mora[1,2,3] | Michael Rzanny[4] | Jana Wäldchen[3,4] | Hannes Feilhauer[1,2,3] | Teja Kattenborn[5] | Guido Kraemer[1,2] | Patrick Mäder[3,6,7] | Daria Svidzinska[1,2] | Sophie Wolf[1,2] | Miguel D. Mahecha[1,2,3,8]

[1]Institute for Earth System Science & Remote Sensing, Leipzig University, Leipzig, Germany; [2]Remote Sensing Centre for Earth System Research, Leipzig University, Leipzig, Germany; [3]German Centre for Integrative Biodiversity Research (iDiv) Halle-Jena-Leipzig, Leipzig, Germany; [4]Max Planck Institute for Biogeochemistry, Jena, Germany; [5]Department for Sensor-Based Geoinformatics, University of Freiburg, Freiburg, Germany; [6]Data Intensive Systems and Visualisation, Technische Universität Ilmenau, Ilmenau, Germany; [7]Faculty of Biological Sciences, Friedrich Schiller University, Jena, Germany and [8]Center for Scalable Data Analytics and Artificial Intelligence (ScaDS.AI Dresden/Leipzig), Leipzig, Germany

Correspondence
Karin Mora
Email: karin.mora@uni-leipzig.de

Funding information
Saxon State Ministry for Science, Culture and Tourism (SMWK), Grant/Award Number: 3-7304/35/6-2021/48880; iDiv funded by the German Research Foundation, Grant/Award Number: DFG-FZT 118 and 202548816; Bundesministerium für Bildung und Forschung, Grant/Award Number: 01IS20062; Bundesministerium für Umwelt, Naturschutz, Bau und Reaktorsicherheit, Grant/Award Number: 3519685A08 and 3519685B08; Thuringian Ministry for Environment, Energy and Nature Conservation, Grant/Award Number: 0901-44-8652; Deutsche Forschungsgemeinschaft, Grant/Award Number: 444524904 and 504978936; Deutsches Zentrum für Luft- und Raumfahrt, Grant/Award Number: ML4Earth; iDiv Flexpool, Grant/Award Number: 346001237; Volkswagen Foundation, Grant/Award Number: 9B937; Alexander von Humboldt-Stiftung, Grant/Award Number: 232201751

Handling Editor: Si-Chong Chen

Abstract

1. Phenological shifts across plant species is a powerful indicator to quantify the effects of climate change. Today, mobile applications with automated species identification open new possibilities for phenological monitoring across space and time.
2. Here, we introduce an innovative spatio-temporal machine learning methodology that harnesses such crowd-sourced data to quantify phenological dynamics across taxa, space and time. Our algorithm links individual phenological responses across thousands of species and geographical locations, using a similarity measure. The analysis draws on nearly ten million plant observations collected through the AI-based plant identification app Flora Incognita in Germany from 2018 to 2021.
3. Our method quantifies changes in synchronisation across the annual cycle. During the growing season, synchronised behaviour can be encoded by a few characteristic macrophenological patterns. Nonlinear spatio-temporal changes of these patterns can be efficiently quantified using a data compressibility measure. Outside the growing season, the phenological synchronisation diminishes introducing noise into the patterns.
4. Despite biases and uncertainties associated with crowd-sourced data, for example due to human data collection behaviour, our study demonstrates the feasibility of deriving meaningful indicators for monitoring plant macrophenology from individual plant observations. As crowd-sourced databases continue to expand, our approach holds promise to study climate-induced phenological shifts and feedback loops.

KEYWORDS
citizen science, Isomap, machine learning, macroecology, macrophenology, nonlinear dimension reduction, plant phenology, spatio-temporal dynamics

1 | INTRODUCTION

Phenology analyses the plant response to climatically driven seasonal variability (Menzel et al., 2020; Piao et al., 2019). Multiple plant physiological metrics for characterising plant phenological conditions are routinely applied. At the plant level, observations such as bud-burst, leaf-out or flowering are recorded to understand phenological shifts across years or over geographical space. National institutions such as the German Weather Service (DWD) oversee phenological networks that mobilise citizen scientists to document local-level phenological changes across broader regions (Renner & Chmielewski, 2021). These networks systematically collect extensive, long-term data sets through the contributions of thousands of trained volunteers adhering to well-defined protocols. Nevertheless, a persistent decline in the number of volunteers over several years poses a substantial risk to data accuracy, affecting not only German but also other networks (Yuan et al., 2021). Phenological gardens are widespread but sparsely distributed and, and are partly hosted by meteorological or long-term ecological monitoring networks (Renner & Chmielewski, 2021). They follow meticulous sampling protocols, partly requiring cloned species to exclude the effect of biological adaptation. This large effort necessarily leads to sparse observation networks.

Near surface sensing such as PhenoCams, that is digital cameras that monitor vegetation, have emerged as a much less labour-intensive, yet also a less detailed alternative. They essentially record integrated vegetation phenological stages across a range of ecosystems (see e.g. Richardson et al., 2018). Although these monitoring approaches are of high temporal quality and resolution, their global distribution is likewise sparse, lacking spatial continuity between observation sites. A systematic approach for ground measurements is prohibitively expensive and thus will always remain limited in spatial and temporal range. Here, we examine to which extent opportunistic data collection through mobile applications can be considered a useful alternative (Moles & Xirocostas, 2022).

Today, mobile phone applications have the potential to significantly enhance the spatio-temporal resolution and coverage of plant observations. The phenological observations are made by citizens who collect individual plant observations. First studies have reported successful usage of smartphone data for deriving phenological metrics of crops (Hufkens et al., 2019), shrubs and trees (Barve et al., 2020), and herbaceous species (Katal et al., 2023; Klinger et al., 2023; Rzanny, Mäder, et al., 2024). However, these studies have to develop new methods to derive phenological information from data collected by smartphone applications, which are typically not tailored for this purpose, but rather developed for species identification. Examples are iNaturalist (Unger et al., 2021), Pl@ntNet (Goëau et al., 2013), Flora Incognita (Mäder et al., 2021), to only name a few. Overviews of these applications are given by Jones (2020) and Katal et al. (2022), illustrating the fast recent developments. Using Flora Incognita, Mäder et al. (2021) and Rzanny, Mäder, et al. (2024) showed that once sufficient data on one species are recorded, the time stamp of the recording offers a good indicator for species phenological conditions. There are two main factors for this phenomenon. First, the application's automatic recognition capabilities are optimised for plants in a flowering state (Rzanny et al., 2019). Second, flowering or fruiting plants tend to be more visually appealing making them more likely to be photographed and identified (Katal et al., 2023; Klinger et al., 2023).

Studies analysing plant phenology, whether through field observations or crowd-sourced data, typically focus on a limited number of species (Alecrim et al., 2023; Katal et al., 2023; Klinger et al., 2023; Miller et al., 2023; Puchałka et al., 2022; Rzanny, Mäder, et al., 2024). However, it remains a challenge to link the individual phenological response across taxa, spatial scales and a variety of ecosystems (Gallinat et al., 2021; Piao et al., 2019). Although, remote sensing monitors an integrated surface phenology at large scales, there is limited information on the dynamics of individual species observations (Gallinat et al., 2021) and it is challenging to link it to ground observations (Tian et al., 2021). Macrophenology is an emerging field that adopts a macroecological perspective (Brown & Maurer, 1989; McGill, 2019) on phenology (Gallinat et al., 2021). The term was first introduced by Doi et al. (2017) and defined as an 'approach to study phenological responses to ongoing climate change at broad scales using tools and theories developed in macroecology'. Here, we build on this idea to derive integrated phenology for plant communities or entire ecosystems. Our idea is to offer a link between remote sensing (Carl et al., 2013; Tian et al., 2021; Wagner, 2021; Zeng et al., 2020; Zhang et al., 2003) and individual plant observations, by retaining a species-specific approach, while at the same time studying the integrated phenology across taxa, time and space.

How can macrophenological dynamics be derived from opportunistically sampled occurrence data? Our fundamental premise is that coherent patterns can emerge from the group behaviour of species occurrences, which have been shaped by shared evolutionary and biogeographic processes (Almeida-Neto & Lewinsohn, 2004) and as a result often exhibit significant redundancy. In the static case, that is where time does not factor in, indirect ordination methods (also referred to as dimension reduction methods, Legendre & Legendre, 2012) have proven successful in extracting such underlying patterns (Mahecha et al., 2007, 2021; Mahecha & Schmidtlein, 2008; van der Maaten et al., 2012). In essence, the authors derive biogeographic gradients from species co-occurrences. They reduce the species dimension, which can be of the order of thousands, by measuring similarities across geographical sampling locations. This spatial similarity structure is represented by a few

characteristic patterns, that is a low-dimensional representation of spatial ecological gradients. In the dynamic case, the same method has been employed to detect collective animal behaviour, such as fish schools, where the movement of individuals converge to create a group dynamic (Abaid et al., 2012; DeLellis et al., 2014). Theoretical experiments involving agent-based models further bolster the notion that group behaviour, which is characterised by low-dimensional coherent patterns, can be discerned through these methods (Abaid et al., 2012; Gajamannage et al., 2015).

Here, we asked whether we can use the temporal detection information across the full range of species recorded with mobile applications to describe macrophenological dynamics. We propose a novel macrophenological approach, which reveals integrated phenological dynamics from the group behaviour of individual plant observations. Specifically, we analysed crowd-sourced observations of plant occurrences and their time-stamp information using the nonlinear dimension reduction method *isometric feature mapping* (Isomap) (Tenenbaum et al., 2000). Robustness is ensured through our temporal data aggregation procedure, and its analysis involves examining the relationship between temporal changes in group behaviour and observation counts.

2 | MATERIALS AND METHODS

2.1 | Data

2.1.1 | Flora Incognita

The Flora Incognita (FI) smartphone application https://floraincognita.com allows users to identify plants directly in the field. The process is based on automatic image classification of one or more images aided by the botanical, geographical and climatic context of the observation (Mäder et al., 2021; Wittich et al., 2018). Currently, the application can identify more than 30,000 vascular plant species, with a strong focus on the flora of Central Europe. An evaluation of identification accuracy when the app was published revealed that 93% of the inspected observations were correct (Mäder et al., 2021). Since then, the identification model has been continuously improved and now achieves an accuracy of >95% for Central European wild flowering plant species (Rzanny, Bebber, et al., 2024). Although poor-quality images may impact individual observations, app-based species identification is typically as accurate or exceeds expert judgement. In contrast to targeted phenological observations, the FI app does not comprise a protocol for phenological studies, is not focused on the recording of phenological data, and is primarily used by botanical laypersons without any prior botanical knowledge. Species are predominantly identified by their most distinct feature, in particular flowers or fruits (Katal et al., 2023; Mäder et al., 2021). Here, we focus on the active phenological state and do not distinguish between flower, leaf or fruit as the goal of our macrophenological approach is to analyse phenology across as many taxa as possible. For this purpose, we employ presence-only binary data, that is 1 = observed active phenological state and 0 = no information. In this analysis, a FI observation consists of the name of the species, the grid cell (location) and the date of the observation (Mäder et al., 2021). This analysis uses 9,759,894 observations collected throughout the period April 2018 (launch) to end of 2021 in Germany. During this period, a total of 2820 plant species were observed.

2.1.2 | Human population density

The number of observations collected with FI have been shown to depend on the human population density, when time is not taken into account (Mahecha et al., 2021). To analyse whether we observe the same effect across time, we employed human population data from the most recent German National Census 2011, provided by the Federal Statistical Office (2011).

2.2 | Spatio-temporal approach to macrophenological dynamics

The spatio-temporal species occurrence is not random but a response to biogeographic processes and driven by seasonal weather and biological dynamics (e.g. herbivory, plant competition and pollination). This is the basis for our assumption that the occurrence of active phenological states embeds and represents inherent information on environmental gradients and seasonal changes. We propose that the phenological group behaviour across time exhibits low-dimensional characteristic patterns, which can be extracted by nonlinear dimension reduction methods. Specifically, we derive macrophenological patterns and measures from opportunistically crowd-sourced occurrence data.

Our approach, visualised in Figure 1, is as follows. In the preprocessing step, these data were aggregated into a grid. We generated a time series of FI occurrence data per grid cell (location ℓ), which serves as an indicator of observable phenological states in Germany. The simultaneously active phenological states are aggregated in discrete time steps using a sliding window approach to diminish temporal bias. We employed the dimension reduction method Isomap (Tenenbaum et al., 2000) per time step, with the aim to reduce up to approximately 3000 species to a few characteristic patterns. These characteristic patterns are referred to as macroecological patterns (MEPs), introduced by (Mahecha et al., 2021) and are combined to form a time series referred to as a macrophenological series (MPS). We computed the residual variance (RV) to estimate data compressibility per time step. To quantify temporal changes in MEPs between two consecutive time steps, we used canonical correlation analysis (CCorA) (Legendre & Legendre, 2012).

In the following section, we first explain how the time series was generated, second how Isomap was adapted and employed, and third how the CCorA was utilised. The analysis was performed with the software R (R Core Team, 2020, version 3.6.3).

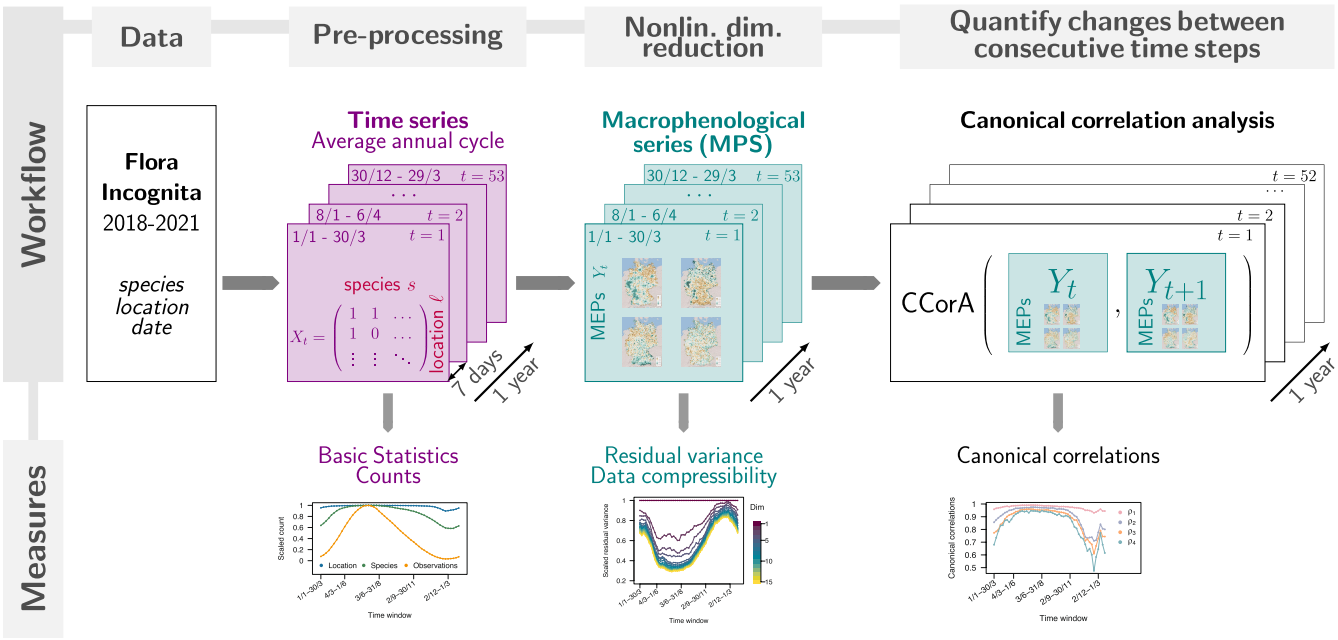

FIGURE 1 The spatio-temporal analysis follows three steps. (1) Pre-processing: We aggregated daily plant occurrence observations from the FI data to represent a time series of an average annual cycle. Per time step t the simultaneous occurrences over 90-day long time windows were gathered, i.e. [1/1–30/3]. Per time step the observation, species and location (grid cell) counts across Germany were determined. (2) Nonlinear dimension reduction (Nonlin. dim. reduction) with Isomap of up to 3000 species per time step t was performed. This gives rise to the macroecological patterns (MEPs). The time series of MEPs is referred to as a macrophenological series (MPS). The residual variance quantifies the data compressibility. (3) We computed the common patterns of consecutive time steps with canonical correlation analysis. Temporal changes between t and $t+1$ were quantified by the canonical correlations. Finally, we study the relationship between the residual variance (RV), canonical correlations and counts, i.e. a proxy of human data collection behaviour.

2.2.1 | Pre-processing: Time-series aggregation

In the pre-processing step, all data sets, that is FI observations and human population counts, were aggregated using the spatial grid employed by (Mahecha et al., 2021). This grid was chosen to maintain continuity with previous national plant surveys (Kühn et al., 2004; Mahecha et al., 2021). Each grid cell is the size of 10′ (arc-minutes) longitude ×6′ latitude, which corresponds to a surface area of approximately 130 km^2, and referred to as location ℓ. The observations density is relatively high due to the high data volume for the chosen grid, and no gap filling or interpolation methods were applied throughout the paper to generate the maps. Our macrophenological approach can be easily adapted to any grid type, provided it is not affected by large observation gaps, that is multiple adjacent grid cells without observations.

The FI data were collected daily over multiple years (2018–2021) and temporally aggregated to represent a time series of an *average annual cycle* by using overlapping time windows (Figure 1). At each time step t a binary matrix $\mathbf{X}_t \in \{0,1\}^{\ell \times s}$ with ℓ locations and s species was generated from FI records. Each matrix $\mathbf{X}_t$ is comprised of observations across a time window of 90 days with consecutive time windows being seven days apart. The sequence of time windows are shown with the date format day/month: {1/1–30/3, 8/1–6/4, … 30/12–29/3}. We obtained a total of 53 time steps (with $t = 1, \ldots, 53$), corresponding to the weeks of the year, Figure 1. For simplicity, we also refer to some time windows with the corresponding name of the meteorological season, that is spring (Spr) ≈ [4/3–30/3] corresponds to $t = 10$, summer (Sum) ≈ [3/6–31/8] corresponds to $t = 23$, autumn (Aut) ≈ [2/9–30/11] corresponds to $t = 36$, and winter (Win) ≈ [2/12–1/3] corresponding to $t = 49$. For simplicity we refer to the period spring—autumn as growing season, and autumn—spring as non-growing season. Overall, across Germany the number of species s and observation locations ℓ fluctuate periodically across the annual cycle, that is $s \in [1622, 2782]$ and $\ell \in [2684, 2991]$ with scaled values in Figure 2c.

With a 90-day time window, we aim to span the duration of a season, while also keeping observation gaps, which could otherwise affect the dimension reduction results, to a minimum. Specifically, in Figure 2c, we show that the scaled number of locations remains above 89.7% throughout the annual cycle, and above 99.0% for 33 out of 53 time steps. Moreover, this window size mitigates the impact of human data collection behaviour, that is no increased observations peaks due to weekends or holidays are observed, Figure 2c. It also accounts for local intra-specific asynchrony in phenological conditions (Almeida-Neto & Lewinsohn, 2004). We also performed computations with a 45-day time window, which are presented in Appendix S5. The seven-day progression was chosen to mitigate human behaviour bias due to the human seven-day rhythm.

In Figure 2a, we show that the observation distribution varies in time and can be concentrated around more densely populated areas, for example in winter Figure 2b. This motivated the analysis to quantify the effects of human population density on Isomap results.

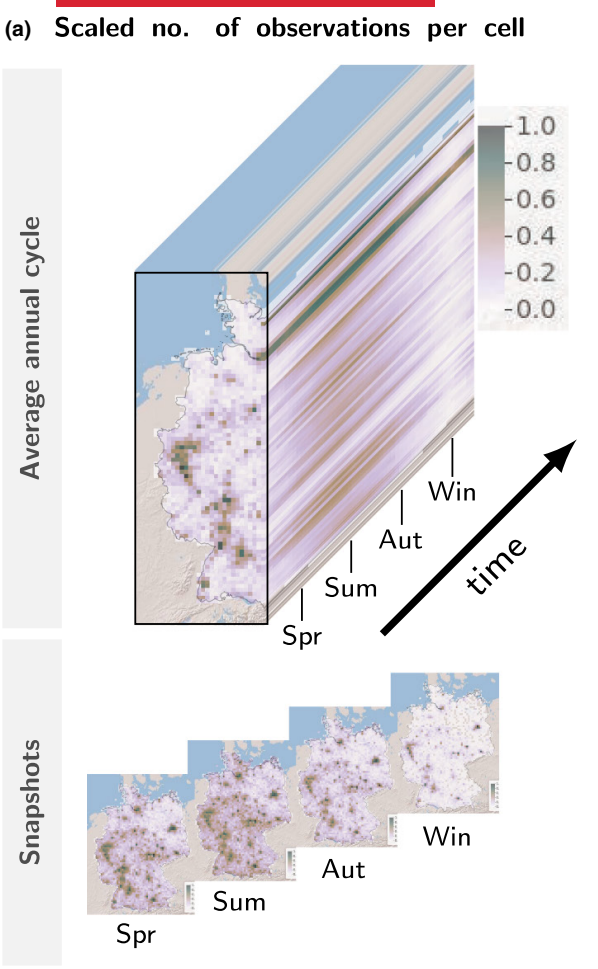

FIGURE 2 Pre-processed data: (a) The number of observations per time step and per grid cell, which where scaled by the maximum per time step (for visualisation only, not part of this analysis). (b) The human population density (number of persons per grid cell) appears to affect observations in (a). (c) Observation counts: the scaled number of total observations, distinct species, and locations (grid cells) across Germany per time step. The counts have been scaled by their respective annual maximum (Appendix S1). The curves indicate periodic but asymmetric behaviour.

Moreover, the 90-day time window captures a majority of the species throughout the average annual cycle indicating data robustness. The shape of the seasonal curves in Figure 2c indicate that fewer total observations do not imply fewer species detected, for example with 50% of the total maximum observations (before [26/02–25/05] and after [29/07–26/10]) we still observe more than 90% of the maximum number of distinct species.

In addition, as a reference to the data compressibility potential, comparable to the results by Mahecha et al. (2021), we aggregated a single and static FI matrix $\mathbf{X}_{\mathrm{FI}} \in \mathbb{R}^{2992\times2820}$, with all species occurrences during the full period 2018–2021, that is no temporal changes are included. As certain species occur only in certain time windows, this static matrix has different dimension s and ℓ to the time series of matrices.

2.2.2 | Nonlinear dimension reduction with isometric feature mapping

Isometric Feature Mapping (Isomap) is a manifold learning or nonlinear dimension reduction method (Tenenbaum et al., 2000), which is also referred to as an indirect ordination in the ecology community. We assumed that in similar biogeographical locations, many species behave similarly, that is the exhibit active phenological states during the 90-day observation time window. Thus, we expected that the phenological group behaviour can be approximated by a few patterns, that is the number of species s (up to 2782 species per time step t) can be approximated by p ($\ll s$) Isomap components. This allows us to analyse group behaviour and compute macrophenological patterns from individual observations across time. Isomap is a nonlinear extension of classical multi-dimensional scaling (Legendre & Legendre, 2012), which aims to detect a low-dimensional manifold $\mathbf{Y}$ embedded in high-dimensional data $\mathbf{X}$, by preserving the local as well as the global manifold structure, that is grid cells with similar species co-occurrence remain close and dissimilar ones remain far away. Below, we give a high-level description of the adapted Isomap algorithm.

First, Isomap constructs a geometric representation, that is a graph, of the phenological group behaviour at time t by quantifying the species co-occurrence similarity between locations i and j with observations $\mathbf{X}^t_{i\star}$ and $\mathbf{X}^t_{j\star}$ where $i,j = 1, \ldots, m$ using the Jaccard distance d_J

$$d_J\left(\mathbf{X}^t_{i\star}, \mathbf{X}^t_{j\star}\right) = 1 - \frac{\left|\mathbf{X}^t_{i\star} \cap \mathbf{X}^t_{j\star}\right|}{\left|\mathbf{X}^t_{i\star} \cup \mathbf{X}^t_{j\star}\right|} \in [0,1], \quad (1)$$

where the notation $\mathbf{X}^t_{i\star}$ refers to row i. From this, the symmetric dissimilarity matrix $\mathbf{D}_J \coloneqq d_J\left(\mathbf{X}^t_{i\star}, \mathbf{X}^t_{j\star}\right)_{ij} \in \mathbb{R}^{\ell\times\ell}$ is constructed. The Jaccard distance is an intuitive replacement for the typically employed Euclidean distance to deal with binary data first proposed for Isomap by Mahecha et al. (2007). Alternative dissimilarity measures (Mainali et al., 2022) can be explored in future work. From the dissimilarity matrix $\mathbf{D}_J$ an undirected neighbourhood graph is constructed, where the graph vertices represent the geographical locations and the graph edges the dissimilarity measure between the corresponding locations, d_J. The neighbourhoods are approximated using the k-nearest-neighbour approach, i.e. k locations (vertices) with the most similar species composition are connected. We chose $k = 16$ for consistency with previous results (Mahecha et al., 2021).

Second, the geometry of the similarity structure of the species co-occurrence is preserved by using the geodesic distance, that is the distance between two points along a curved manifold. The geodesic distance is approximated by computing the shortest path of the graph.

Last, the p-dimensional embedding manifold is constructed with classical Multidimensional scaling (cMDS), such that the geometry of the intrinsic space preserves the geometry of the original co-occurrence data space.

This study focuses on the four leading Isomap components $\mathbf{Y}^t \in \mathbb{R}^{\ell,p}$ with $p = 4$ per time step t, which have been shown to explain most of the variance Mahecha et al. (2021). Each Isomap component per time step is visualised across Germany, Figure 3 (see Appendix S2 for alternative visualisation). They represent environmental gradients, which are referred to as empirical macroecological pattern (MEP) and were first introduced by Mahecha et al. (2021). Consequently, per time step MEPs represent sub-manifolds of the underlying manifold (Gajamannage et al., 2015; Gajamannage & Bollt, 2017), that is snapshots of the underlying macroecological gradients.

The four leading MEPs were assembled into a time series covering the annual cycle, $\left\{\mathbf{Y}^1, \mathbf{Y}^2, \ldots, \mathbf{Y}^{53}\right\}$, which we refer to as the macrophenological series (MPS), as they represent macrophenological changes. As the MEPs are invariant with respect to direction, we used the cosine of the angle among MEPs of consecutive time steps to make them unidirectional.

The residual variance (RV), which quantifies the proportion of data not represented by the respective Isomap components (Tenenbaum et al., 2000), was used to determine approximation quality and data compressibility. The idea is that group behaviour is characterised by low-dimensional manifolds. A similar approach was employed by Abaid

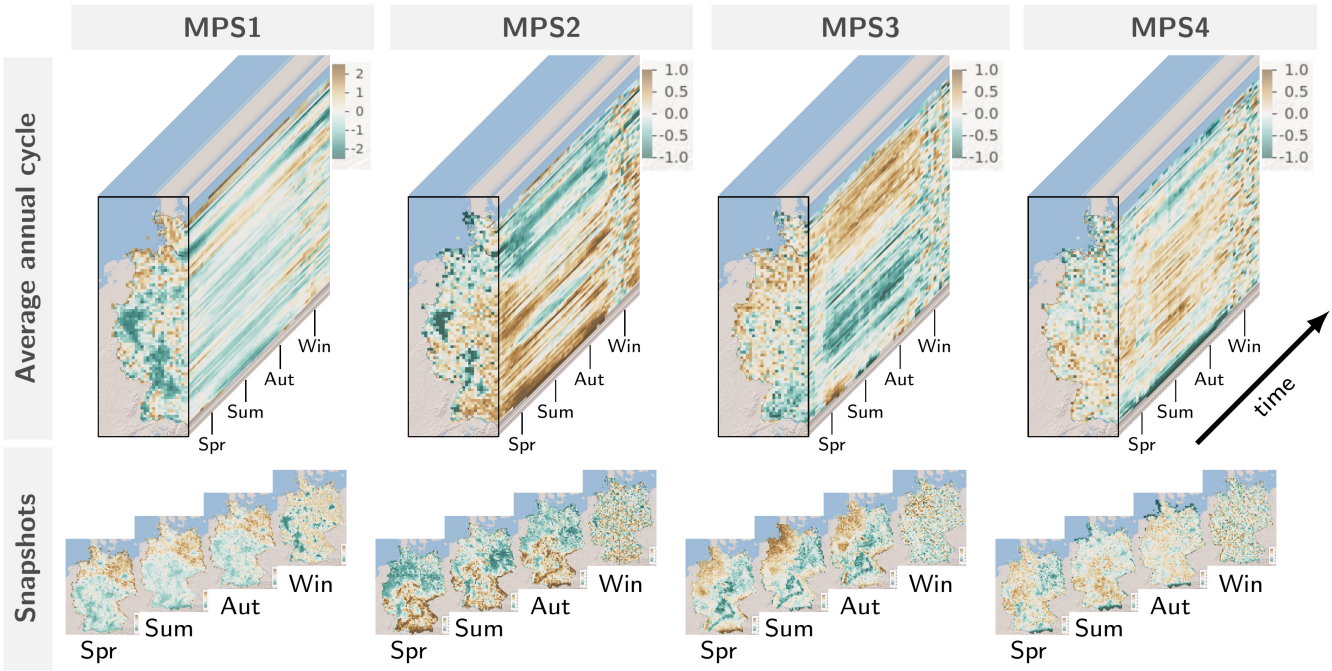

FIGURE 3 Macrophenological series (MPS) across one average annual cycle. They are assembled from the four leading Isomap components, referred to as macroecological patterns (MEPs), per time step. Each MEP, i.e. each map, indicates how similar plant co-occurrence is among grid cells per 90-day time window, that is plant behaviour. Similar group behaviour of plants is indicated by similar colours. The MPS reveal two phases. In phase I characteristic patterns and local changes are observed during the growing season, e.g. Alpine region switches colours in MPS3. In phase II these patterns deteriorate and become noisy indicating a decline in the group behaviour during the non-growing season. Snapshots are a selection of MEPs: the MEPs of the corresponding meteorological season are shown, that is spring (Spr) ≈ [4/3–30/3], summer (Sum) ≈ [3/6–31/8], autumn (Aut) ≈ [2/9–30/11], winter (Win) ≈ [2/12–1/3]. Legend: the colour bar indicates the values of the corresponding MEP vector. The first MEP, which explains most of the variance, has the largest value range.

et al. (2012); Gajamannage et al. (2015), who used data generated by agent-based models to demonstrated that RV increases as group behaviour in a single species deteriorates. For a comparison of RV among the time steps, we computed the scaled residual variance (sRV), that is scaled by the residual variance at dimension one (Appendix S3).

The Isomap algorithm was implemented in R and follows the set up of Kraemer et al. (2018, with a general overview of dimension reduction methods).

2.2.3 | Common patterns with canonical correlation analysis

Canonical correlation analysis (CCorA) computes multivariate correlations between two data matrices, $\mathbf{Y}_1$ and $\mathbf{Y}_2$ (Legendre & Legendre, 2012). With CCorA, we analysed temporal changes between the five leading MEPs of consecutive time steps, that is $\mathbf{Y}_1 = \mathbf{Y}^t \in \mathbb{R}^{\ell \times 5}$ and $\mathbf{Y}_2 = \mathbf{Y}^{t+1} \in \mathbb{R}^{\ell \times 5}$, which is denoted $\mathrm{CCorA}\left(\mathbf{Y}^t, \mathbf{Y}^{t+1}\right)$ for $t = 1, \ldots, 53$. Canonical variates (CVs), which are linear combinations of the respective MEPs, represent common patterns between the two MEPs $\mathbf{Y}^t$ and $\mathbf{Y}^{t+1}$ and will be referred to as such. The strength of the linear relationship among canonical variates is measured by the canonical correlation ρ. Here, it quantifies how much MEPs have changed from one time step to the next. Explicitly, CCorA seeks coefficients $\mathbf{a}_1 \in \mathbb{R}^5$ and $\mathbf{b}_1 \in \mathbb{R}^5$, which maximise the canonical correlation ρ_1 between the linear combinations $\mathbf{z}_1^{(1)} := \mathbf{Y}_1\mathbf{a}_1$ and $\mathbf{z}_2^{(1)} := \mathbf{Y}_2\mathbf{b}_1$ of matrices $\mathbf{Y}_1$ and $\mathbf{Y}_2$, respectively,

$$\rho_1 = \mathrm{corr}\left(\mathbf{z}_1^{(1)}, \mathbf{z}_2^{(1)}\right). \tag{2}$$

The vectors $\mathbf{z}_1^{(1)}$ and $\mathbf{z}_2^{(1)}$ are referred to as the first CV pair. The subsequent CV pairs $\mathbf{z}_1^{(i)}$ and $\mathbf{z}_2^{(i)}$ with $i = 2, \ldots, 5$ are sought in a similar way but are subject to the constraint that new pairs are uncorrelated to the previous ones, that is each CV matrix $\mathbf{Z}_1 = \left[\mathbf{z}_1^{(1)}, \mathbf{z}_1^{(2)} \ldots, \mathbf{z}_1^{(5)}\right] \in \mathbb{R}^{\ell \times 5}$ and $\mathbf{Z}_2 = \left[\mathbf{z}_2^{(1)}, \mathbf{z}_2^{(2)} \ldots, \mathbf{z}_2^{(5)}\right] \in \mathbb{R}^{\ell \times 5}$ is orthogonal. The corresponding canonical correlations are given by $\rho = \left\{\rho_1, \ldots, \rho_5\right\}$. Above, we assumed that the MEPs $\mathbf{Y}^t$ and $\mathbf{Y}^{t+1}$ cover the same observation locations. When this is not the case, common locations ℓ are selected before performing the CCorA.

Moreover, CCorA was employed to analyse the effects of the human population density $\mathbf{Y}_{\mathbf{pop}}$ on the MPS per time step, that is $CCorA\left(\mathbf{Y}^t, \mathbf{Y}_{\mathbf{pop}}\right)$ for $t = 1, \ldots, 53$.

3 | RESULTS

3.1 | Macrophenological series

Our macrophenological approach with Isomap yields a low-dimensional representation of the group behaviour over the course of an aggregated annual cycle represented by the MPS $\left\{\mathbf{Y}^1, \mathbf{Y}^2, \ldots, \mathbf{Y}^{53}\right\}$ (Figure 3). We visualise the four leading MEPs across the 53 time steps, which represent the thousands of observed plant species (min = 1622, max = 2782 depending on the time step). An alternative to the data cube visualisation is shown in Appendix S2.

The MPS in Figure 3 reveal two main phases. Phase I occurs during the growing season and is characterised by a coherent spatio-temporal pattern, which indicates group behaviour. Phase II occurs during the non-growing season, especially winter, and the coherent patterns deteriorate and become noisy. The absence of patterns signifies that group behaviour is not detectable from occurrence data as the phenological states are not visible to the mobile application. From the ecological perspective, this represents dormancy or death. The transition between the two phases is gradual. During phase I, each MPS is dominated by a distinct and robust characteristic feature, for example MPS1 exhibits a north–south divide in similarity of group behaviour Figure 3. Moreover, it appears to be a near time invariant pattern, this is further quantified in Section 3.4. Overall, all MPS indicate geographic characteristics such as mountain ranges, lowlands, or rivers. In each MPS, local changes can be observed, for example in MPS3, the Alpine region is similar to northeast Germany in spring and autumn, but during summer, it is more similar to central Germany (Figure 3). Overall, certain regions exhibit varying start and end times of group behaviour similarity. In phase II, while MPS2-4 are mostly noisy, MPS1 distinguishes group behaviour similarity between regions with high (dark teal) and low (brown) human population density, for example winter in Figure 3.

3.2 | Temporal changes in residual variance indicate changes in data compressibility

We analysed the data compressibility at each time step. The sRV quantifies the proportion of data points that is not represented by the respective MEPs. At the same time, it indicates how well the data can be compressed.

To gain an intuition for the temporal changes in the residual variance, we compared the sRV of five time windows and the static FI data (Figure 4a). The sRV varies among time windows. It exhibits the most rapid decline and to lower values in the static FI data alongside the meteorological spring ≈ [4/3–30/3] and summer ≈ [3/6–31/8] (Figure 4a). This suggests a superior approximation and greater compressibility in comparison with the other time windows (autumn ≈ [2/9–30/11], winter ≈ [2/12–1/3], and [1/1–30/3]). Heuristically, the minimal suitable number of MEPs necessary to represent the flowering occurrence (embedding dimension p), is determined by the 'elbow' in the sRV curve as the dimension increases, that is the dimension at which the curve's slope flattens. During the non-growing season this elbow feature is less pronounced and the sRV remains high across 15 dimensions, for example for autumn ≈ [2/9–30/11], winter ≈ [2/12–1/3], and, [1/1–30/3] (Figure 4a).

The temporal changes in the sRV across the annual cycle are gradual (Figure 4b). Here, the elbow feature is indicated by the absence

of gaps between the curves. Although the embedding dimension p varies across time, higher dimensions (> 4) do not explain substantially more variance, validating our focus on the four leading MEPs ($p = 4$) in this study. Overall, the sRV curves for all dimensions have a periodic yet asymmetrical shape, that is the slopes in early spring period are steeper than in the autumn period (Figure 4b). The spring–summer transition is characterised by a relatively high and constant sRV. Both, the low sRV and the low embedding dimension of $p = 4$, indicate a high data compressibility. We interpret this as group behaviour, which reflected in the corresponding MPS exhibiting coherent patterns (Figure 3). Between autumn and early spring, the high sRV indicates that these data are difficult to compress and that all 15 components do not represent the occurrence data well. During this phase, the corresponding MPS are noisy and structureless (Figure 3), reflecting the absence of group behaviour detectable in occurrence data.

3.3 | Seasonal transitions: Data compressibility vs. observation counts

We analysed how the temporal changes in scaled residual variance (Figure 4) are affected by the changes in observation counts across Germany (Figure 2c). We found the cyclical relationship between the sRV and the corresponding counts (Figure 5) to be partly overlapping (deformed cycles). This result is robust across dimensions (Appendix S4).

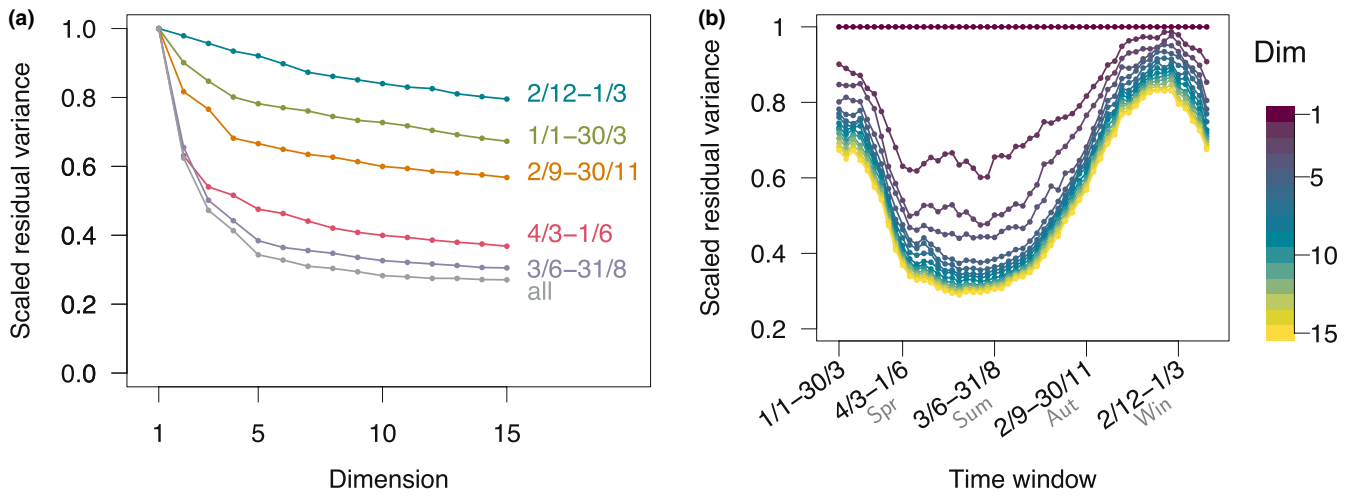

FIGURE 4 Scaled residual variance (sRV) indicates data compressibility, that is low sRV indicates high compressibility and high sRV vice-versa. (a) The sRV of five time windows and static FI data (all) vary. The elbow feature is less distinct toward the end of the annual cycle (orange, green, blue). (b) The sRV curves across the annual cycle for 15 dimensions (colour bar) are plotted here vertically per time step. The curve for dimension 1 is constant, as this is the scaling value. The sRV for dimension 2–15 exhibits a seasonal but asymmetrical cycle. The transition in early spring occurs faster than in autumn.

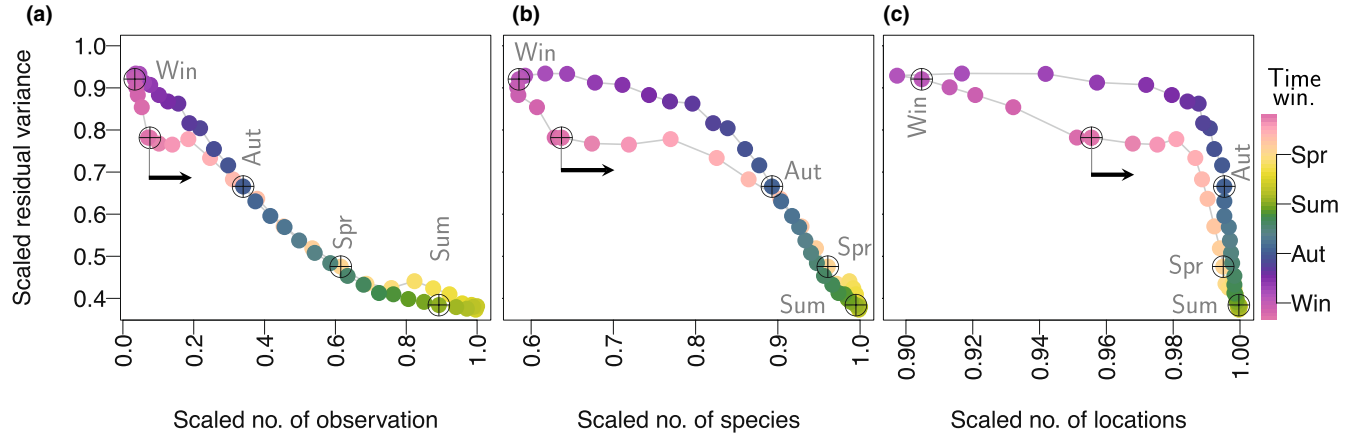

FIGURE 5 Temporal relationship between data compressibility indicated by the scaled residual variance (sRV) for embedding dimension $p = 5$ (from Figure 4b) and the scaled number of observations (a), species (b), and locations (c) (from Figure 2c), respectively. These partly overlapping cycles indicate distinct seasonal differences. Even when the counts are the same, differences in sRV can be observed in pre- and post-winter (dark blue, magenta). The differences pre- and post-summer are minor in comparison (yellow, green).

Overall, we expected similar counts to result in similar sRV, for example as is observed for the period pre-spring to summer (time steps 6–22 or [5/2–4/5]–[27/5–24/8]) and summer to autumn (time steps 23–36 or [3/6–31/8]–[2/9–30/11]), where the data points mostly overlap. This indicates that during these time periods the occurrence data are comparably compressible (Figure 5a,b). Consequently, the quality of group behaviour is very similar at the corresponding time points even if the corresponding MEPs differ.

However, we also show that, even when the counts are the same, the sRV can differ. Specifically, larger values are observed in the autumn–winter period (time windows 37–49 or [9/9–7/12]–[2/12–1/3]), indicating a worse approximation quality and data compressibility, than in the winter–spring period (time windows 50–6 or [9/12–8/3]–[5/2–4/5]) (Figure 5a,b). We also observe that in the winter–spring period, unlike the autumn–winter period, the data points are further apart as the scaled number of species increases, indicating a faster increase in scaled species numbers. In other words, for the same counts, we observe better data compressibility with corresponding coherent, less noisy MPS during the winter–spring transition. This indicates that group behaviour similarity has a seasonal characteristic, which changes gradually and does not seem to dependent on observation counts alone.

We also investigated whether location gaps, resulting from grid cells without observations, affect the approximation quality (Figure 5c). For most of the growing season, the scaled number of locations is above 0.98. It is during this period that approximation quality changes to low residual variance. This is most likely a result of the decreasing total observation and species numbers and not location gaps.

In the following, we remark on specific seasonal transitions in Figure 5. The *spring to summer period* is characterised by the most compressible occurrence data with low sRV of (0.38,0.48) and small variations in species count (0.96,1.00) despite a large variation in scaled observation counts (0.6,1.0). This indicates strong group behaviour. During the *summer to autumn period*, the sRV varies substantially more, that is (0.38,0.67), as a result of a large variation in observations counts (0.3,0.9), while variation in scaled species counts remain low (0.89,1.00). This indicates that towards the end of the period, the flowering behaviour loses its group characteristic and may start to become affected by declining observation numbers. During the *autumn to winter period*, the data are most difficult to compress, that is high sRV in (0.67,0.92). The observation count is low with a small range (0.0,0.3). The scaled species reach their minimum, that is (0.59,0.89). Toward the end of this period, the corresponding MPS lose their coherent patterns. This demonstrates that as long as the scaled observation counts remain above 30%, the underlying environmental gradients give rise to coherent patterns and indicate group behaviour. The coherent pattern in the MPS return during the *winter to spring period*. The occurrence data become more compressible as the scaled sRV (0.48,0.92) decreases with increasing scaled observation (0.0,0.6) and species (0.59,0.96) counts.

Each data point is associated with a time window in the annual cycle indicated by the colour bar. The start of the year is indicated by the arrow, and crosses indicate the time windows corresponding to the meteorological seasons. These annual cycle curves are deformed circles, which partly overlap. Low sRV indicates high data compressibility (group behaviour) and high sRV vice versa.

3.4 | Temporal changes in common MPS of consecutive time steps with canonical correlation analysis

We analysed how much MEPs change between two consecutive time steps t and $t+1$. To quantify these changes, we used canonical correlation analysis, $\mathrm{CCorA}(\mathbf{Y}_t, \mathbf{Y}_{t+1})$. The strength of the linear relationship among CVs, which was measured by canonical correlations $\rho_1, \ldots, \rho_4$, changes in time, (Figure 6). Each CV (Appendix S6) is predominantly associated with the corresponding MEP per time step t (Appendix S7).

Overall, Figure 6 demonstrates that, despite the overlap of 83 days, the MPS capture substantial and rapid changes in the 7 days at the beginning or end of the consecutive time windows. The first canonical correlation remains relatively constant and high, with $\rho_1 \in (0.93, 0.99)$ throughout the annual cycle. The corresponding canonical variates, $\mathbf{Z}_t^{(1)}, \mathbf{Z}_{t+1}^{(1)}$, have a strong linear relationship, which indicates that they are largely time invariant. This indicates that the associated MPS represent processes that are changing little or not at all in time.

In contrast, the other correlation values, ρ_2, ρ_3, ρ_4, exhibit distinct periodic behaviour indicating that the canonical variates and hence the corresponding MPS undergo seasonal changes. The largest and fastest changes are observed during the transitions winter–spring and late summer–winter. During the growing season, we observe the highest correlation, which remains fairly constant. During this

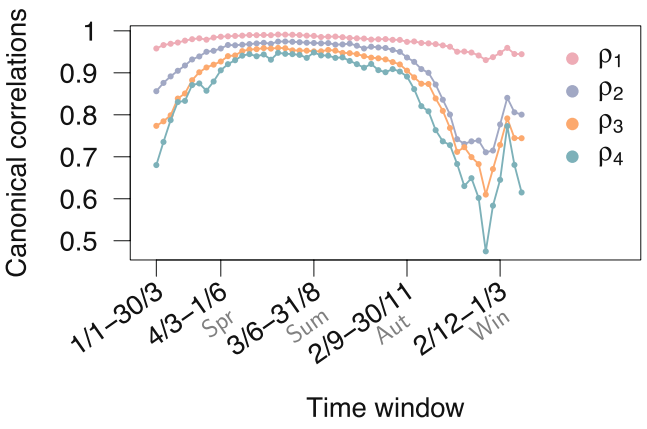

FIGURE 6 Canonical correlations ρ_i for $i = 1, \ldots, 4$ indicate seasonal changes in macroecological patterns between consecutive time steps. High values indicate few changes in macrophenological series as observed during spring—autumn, and vice versa.

period, the canonical variates between consecutive time steps have a strong linear relationship indicating small temporal changes. During the non-growing season, the linear relationship is less strong, reaching a minimum of $\rho_4 = 0.47$ in early winter due to the corresponding noisy MEPs.

3.5 | Seasonal transitions: Canonical correlations of common MPS of consecutive time steps vs. observation counts

We analysed the relationship between the temporal changes between consecutive time steps, measured by the canonical correlations (from Figure 6), and the changes in observation counts across Germany (from Figure 2c). Here, we focus on the canonical correlation ρ_2 (Figure 7), as ρ_1 exhibits only few changes in time, and the results for ρ_3 and ρ_4 are equivalent (Appendix S8).

Overall, the cyclic relationship is comprised of an overlapping and a non-overlapping curve section in the annual cycle (Figure 7), as exhibited by sRV in the previous section. The overlapping curve sections show similar changes in MEPs between consecutive time steps during seasonal transitions. Specifically, the canonical correlation ρ_2 remains above 0.94 despite large variations in the scaled number of observations (0.34 – 1.00), with the scaled number of species remainaining high (0.89, 1.00), during pre-spring–summer (time steps 7–22, i.e. [12/2–11/5]–[27/5–24/8]) as well as during summer-autumn (time steps 23–36, i.e. [3/6–31/8]–[2/9–30/11]). Moreover, the pre-spring MEPs (at $t = 7, 8, 9, 10$) change slightly more than the summer-autumn MEPs as indicated by ρ_2 (Figure 7). This is more pronounced in the canonical correlations ρ_3 and ρ_4 (Appendix S8). Due to the high observation count and good approximation quality (high sRV), we interpret this to indicate a predominantly phenological change.

The non-overlapping curve sections in the annual cycle are characterised by larger variations in scaled total observations and species counts between consecutive time steps (Figure 7). The canonical correlation ρ_2 indicates that the corresponding MPS undergo fewer changes in winter—pre-spring (time steps 49–6, i.e. [2/12–1/3]–[5/2–4/5]) than in autumn—winter (time steps 36–48, i.e [2/9–30/11]–[25/11–22/2]) despite arising from the same scaled total observation and species counts. These seasonal differences indicate that the MEPs and hence the group behaviour deteriorates fast between consecutive time steps from autumn onward and become noisy (low ρ_2). In winter [2/12–1/3] as the group behaviour emerges again the MEPs change slowly once established indicated by slowly increasing ρ_2 (Figure 7).

3.6 | Temporal effects of human population density

The constant human population density in Germany is one factor that appears to affect the observations in time (Figure 2a,b). We analysed how this spatial pattern influences the five leading MPS. To quantify this effect we apply canonical correlation analysis to the two data sets: static scaled human population density $\mathbf{Y}_{pop}$ and the FI macrophenological series per time step $\mathbf{Y}_t$, that is $\mathrm{CCorA}(\mathbf{Y}_{pop}, \mathbf{Y}_t)$

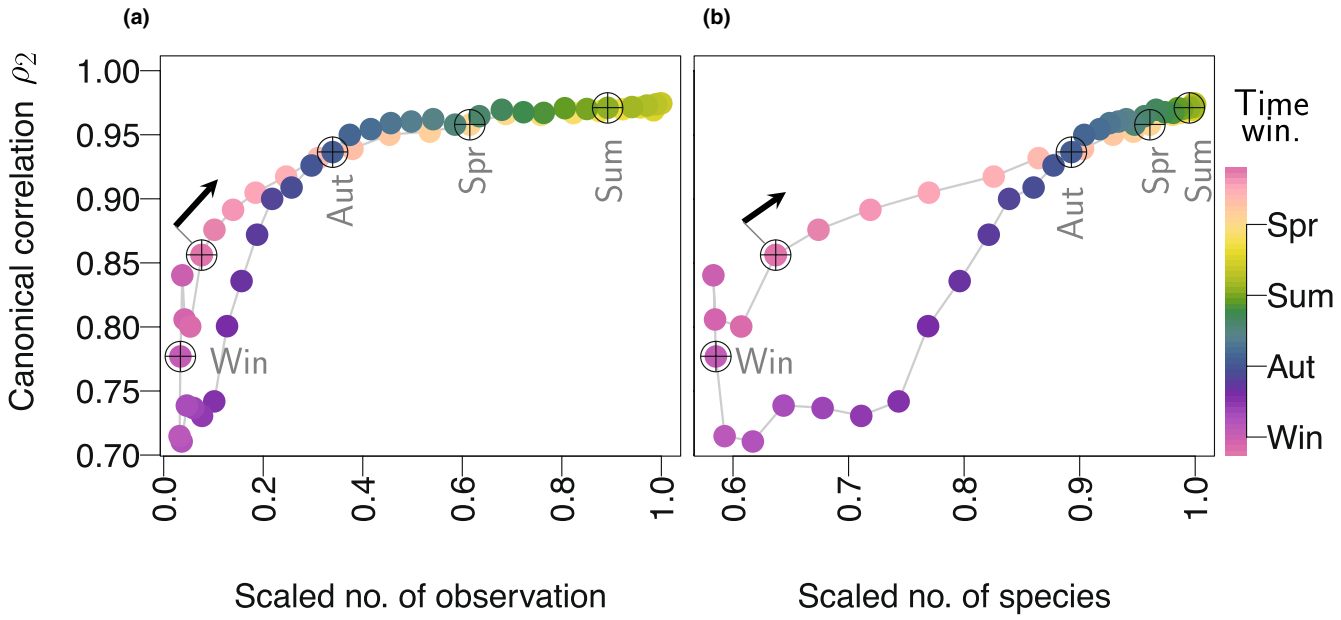

FIGURE 7 Temporal relationship between changes in MEPs between consecutive time steps indicated by canonical correlation ρ_2 (from Figure 6) and scaled number of observations (a) and species (b) (from Figure 2c), respectively. These partly overlapping cycles indicate seasonal differences. Even when the counts are the same, differences in ρ_2 can be observed in pre- and post-winter (dark blue, magenta). The differences pre- and post-summer are minor in comparison (yellow, green). Each data point is associated with a time window in the annual cycle indicated by the colour bar. The arrow indicates the start of the annual cycle, and crosses indicates the time windows corresponding to the meteorological seasons.

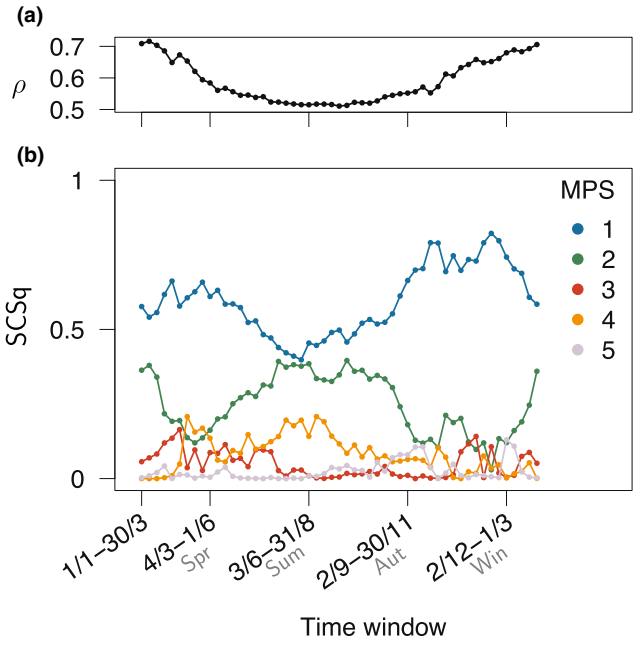

FIGURE 8 Effects of human population density on MPS per time step quantified by canonical correlation analysis $\mathrm{CCorA}\left(\mathbf{Y}_{\mathbf{pop}}, \mathbf{Y}_t\right)$. (a) Canonical correlation (ρ) and (b) structural correlations squared (SCSq) indicate that the largest human population density effect occurs in MPS1 during the non-growing season.

. The temporal changes in the canonical correlations revealed a more pronounced influence of human population density during the non-growing season with $\rho > 0.57$ (Figure 8a). We used the structural correlation squared to quantify the proportion each MPS contributes to the respective canonical variates at time t, Figure 8b. It revealed that MPS1 is most affected by the human population density in comparison with other MEPs, especially during the non-growing season. During the growing season, also MPS2 is influenced, albeit to a lesser extent than MPS1. This indicates that MPS1 isolates the human population density signal component and thus can be viewed as an effective filtering step in this analysis.

4 | DISCUSSION

Our approach shows how our machine learning methodology can overcome the challenge to analyse the phenology of thousands of species across taxa, space, and time. Our study reveals synchronised group behaviour among thousands of plant species across time and the ecosystems they share. This behaviour exhibits an inherent order, which is characterised by coherent patterns (MPS in Figure 3), approximated by nonlinear dimension reduction techniques. Our macrophenological approach provides a macroecological prospective on the phenology of numerous species using individual occurrence observations. This is only possible with a large data set, such as crowd-sourced data from the Flora Incognita app, which covers broad spatial and temporal scales. While our substantial data set of nearly ten million observations offers statistical power, our study makes the entanglement of human data collection behaviour and macrophenology visible and shows the challenges in establishing thresholds between the two. Therefore, it is crucial to interpret these findings cautiously, acknowledging that the reliability of our results and the applicability of this approach in similar contexts depend on the quality of the underlying data.

In the following, we first discuss the capabilities of our macrophenological approach, second disentangling phenology and human behaviour, third the data quality of automated species identification, forth validation and bias, and fifth the potential for future regional to global macrophenology studies.

4.1 | Macrophenological approach

We adopt a complex systems perspective of macroecology, where the co-occurrence among thousands of individual species observations leads to emerging patterns, here represented by the MPS (Figure 3). This approach is combined with the ecology of large-scale systems (McGill, 2019) by covering extensive scales across taxa, space and time. This comprehensive scope enables the definition and examination of macrophenology (Gallinat et al., 2021), here represented by the MPS (Figure 3).

Our findings underscore the feasibility of our approach to describe macrophenological dynamics across an annual cycle. They reveal that a spatio-temporal approach is necessary to fully capture the emergent macrophenological patterns (Figure 3). We showed that our macrophenological approach detects two main spatio-temporal phases in the FI occurrence data: group behaviour during the growing season and absence of group behaviour during the non-growing season. This was quantified by two measures: (i) the MPS revealing gradual transition between coherent and noisy patterns (Figure 3) and (ii) the sRV indicating temporal changes in data compressibility (Figure 4b). We have shown that the MEPs and hence the group behaviour across the average annual cycle changes nonlinearly across time, indicating that group behaviour emerges fast in spring, remains strong over the summer, and declines slowly in autumn when the corresponding patterns become noisy. Our analysis revealed one nearly time invariant and three dynamic MEPs demonstrating that our approach can robustly distinguish between more static (MPS1) and dynamic processes (MPS2-4) (Figure 6). All measures uncovered periodic but asymmetric dynamics with gradual changes. Moreover, these measures consistently detect seasonal differences before time window [12/2–11/5] and after time window [2/9–30/11] as the number of observations and species change (Figures 5 and 7). We propose these time windows as the start and end points of the macrophenological growing season in Germany, which is characterised by group behaviour in the MPS (Figure 3). This definition of growing season requires further comparison with other data sets, which goes beyond the scope of this study.

During the growing season, this dynamics appears robust with respect to the observation counts, that is the data compressibility remains high despite considerable variations in observation counts

(Figure 5). Moreover, the sRV exhibits nearly identical dynamics between the first and the second half of the macrophenological growing season as data counts vary, that is overlapping curve sections in Figure 5. This indicates similar changes in the compressibility of the occurrence network, despite potentially varying human data collection behaviour. This suggests that our approach reveals macrophenological dynamics, which shows signs of symmetry between the first and the second half of the macrophenological growing season.

Outside the growing season, the time series exhibits more varied dynamics. On the one hand, during the winter period, the low observation counts affect data compressibility and thus drive the dynamics, which is characterised by the absence of group behaviour. This could reflect the unobservable phenological states, that is plants are either dormant or dead, or that not enough observations were made to represent the group behaviour in winter. The relation to human behaviour is elaborated on in Section 4.2. On the other hand, when observation counts are approximately the same, seasonal differences in the sRV (Figure 5) and canonical correlations (Figure 7) become evident between the pre- and the post-winter period. Specifically, the group behaviour is stronger post-winter than pre-winter. This indicates that despite approximately the same low observation counts the co-occurrence relations can give rise to group behaviour. This also suggests macrophenological dynamics.

The time window size (TWS) serves not only as a parameter in our algorithm but also as an indicator of the temporal dynamics within the data over a specified period (see Appendix S5). Reducing the TWS to 45 days leads to observations and analysis of different plants. Particularly in spring (see Appendix S5), we observe rapid changes in occurrence, with a noticeable decrease in residual variance of approximately 6–7 weeks (42–49 days) after reducing the TWS, suggesting that the phenological group behaviour among plant species emerges in late spring. Conversely, the phenological transition in late autumn remains comparable between TWS of 45 and 90 days, indicating consistent spatio-temporal species occurrence and phenological group behaviour regardless of TWS. Overall, our method effectively captures the main emerging and ceasing characteristic patterns (MPS) across varying TWS (Appendix S5), underscoring the robustness of our approach. However, it is important to consider the limitations of TWS imposed by data density as well as for interpreting phenological results.

4.2 | Disentangling phenology and human behaviour

Disentangling phenology and human data collection behaviour is a complex challenge. To address this, various steps were taken to mitigate or quantify the effects of human behaviour. Here, we discuss advantages and disadvantages of such approaches and ask to what extent disentangling is possible.

We employed a time-series aggregation procedure in our study to mitigate the potential temporal bias introduced by human data collection behaviour (Binley & Bennett, 2023; Callaghan et al., 2021; Knape et al., 2022; Primack et al., 2023). This approach smoothed the occurrence counts (Figure 2c) in two ways. First, it smoothed the fluctuations in observation counts resulting from human behaviour, such as data collection peaks during weekends (Courter et al., 2013; Knape et al., 2022; Sparks et al., 2008) and holidays (Callaghan et al., 2021; Knape et al., 2022), or fewer observations during extreme weather events. Second, it provided an average occurrence data set, which is not affected by plant individual variability (Almeida-Neto & Lewinsohn, 2004). However, this aggregated time series limits our ability to investigate macrophenology at finer time scales. This limitation is expected to diminish as the database continues to grow.

The low counts observed in winter pose a particular challenge due to their impact on their statistical power. Moreover, it remains unclear to what degree these low counts are driven by the underlying phenological changes, such as a decline in species occurrence, or by data collection behaviour, i.e. a reduction in the species being observed. Possible validation approaches with alternative data sets are discussed in Section 4.4.

Despite our data aggregation, we observed a human population density bias, which appears to be linked to the relatively low observation numbers during the non-growing season (Figure 5). We showed that this bias mainly manifested in one of the leading components (MPS1), especially during the non-growing season. As such, the bias can be considered isolated, and our approach presents an effective filtering (Figure 8). At the same time, MPS1 characterises static processes, of which human population density is one but not the only factor. What other factors underlie the prominence of MPS1? For example, it could be resulting from the distribution of wind-pollinated species (Kühn et al., 2006), which give rise to a similar north–south pattern. What gives rise to the distinct urban–rural pattern non-growing season? Further analyses are needed to understand to what degree MPS1 results from human data collection behaviour, such as citizen scientists going on fewer/shorter excursions during the winter months, and to what extent it is influenced by the greater species richness in urban areas (Kühn et al., 2004), where phenology is impacted by urban heat, artificial light, and pollution (Kühn et al., 2004; Wohlfahrt et al., 2019).

4.3 | Data quality of automated species identification

Opportunistically collected presence-only data typically exhibit temporal, spatial and taxonomical imbalances, resulting in characteristic seasonal patterns (Knape et al., 2022). For species with attractive flowering or fruiting stages, the number of observations increases, when there is a sudden change in the app users identification interests. This is usually the case when those plants start to bloom or fruit. Such species provide a clear signal that can be linked to distinct phenological stages (Katal et al., 2023). However, this is not the case for species with less attractive flowering stages such as

many trees, grasses or sedges, which do not show uniquely attractive stages during their yearly cycle. Generally, such species are less likely to be observed by the app users. These taxonomic biases may lead to a stronger contribution of visually attractive species to the overall phenological signal, but they do not appear to affect annual changes in the observed group behaviour. Evidence for this are the MPS, which are characterised by a consistent and characteristic pattern across the growing season.

4.4 | Validation and bias

Opportunistically collected crowd-sourced data from mobile applications are considered a novel data source (Callaghan et al., 2021) and require the same validation standards as professionally collected scientific data. It was shown that both data sources are subject to very similar biases and errors (Binley & Bennett, 2023).

One of the main differences between crowd-sourced and traditional scientific data is the sampling strategy. Data collected with mobile applications are opportunistic and partly driven by human behaviour, while traditional large scale data collections are considered more systematic. Overall, analyses of mobile application data have shown to yield comparable results to systematically collected data (Katal et al., 2023; Klinger et al., 2023; Mahecha et al., 2021; Schiller et al., 2021; Wolf et al., 2022). For example, Wolf et al. (2022) have shown good agreement of plant trait maps derived from iNaturalist (global coverage) with the scientifically collected sPlotOpen data set (regional coverage).

In the static case, the Flora Incognita data set was shown to be in high agreement with the more systematically collected data set FlorKart, the German inventory of vascular plant occurrences in Germany (Mahecha et al., 2021). To find an appropriate reference data set for phenological comparisons with the Flora Incognita data, which encompasses the same spatial and temporal coverage, remains a challenge (Katal et al., 2023). One future validation avenue could explore the relationship between our macrophenological approach and the macrophenology derived from satellite observations, for example (Purdy et al., 2023; Studer et al., 2007; Tian et al., 2021; Zeng et al., 2020; Zhang et al., 2003).

4.5 | Outlook: Potential for regional to global macrophenology studies

Our methodology is scalable, making it in principle suitable for applications across a wide range of spatial scales and for data of much higher spatio-temporal resolutions. This versatility allows for its effective deployment, whether at the local level, such as in grid-based plot studies in controlled experiments, or on a global scale. At the local scale, our macrophenological approach can be adeptly employed to describe and characterise plant communities within specific study sites. Focusing on regional flowering data our approach could explore phenological dependencies between plants and pollinators. Conversely, at the global scale macrophenological patterns could be extracted from crowd-sourced data such as iNaturalist (Unger et al., 2021), Pl@ntnet (Goëau et al., 2013), or The Global Biodiversity Information Facility (2023) to name only a few. These have the potential to analyse biodiversity and discern the drivers behind biogeographic processes, all derived from individual observations.

We have shown that regional changes in MPS occur at different rates and different points in time Figure 3. For example, group differences in mountainous regions versus lowlands are pronounced in spring and autumn but level out during summer in MPS2. These changes could represent the varied response to the local microclimate as well as the feedback loop of the microclimate shaping vegetation and vice versa, (Kemppinen et al., 2023). These results are in line with the study by Rzanny, Mäder, et al. (2024), who showed that opportunistically collected data of 20 species reveal shifts in flowering phenology across Europe, particularly accentuated for spring-flowering species, with elevational shifts of 6–17 days per 1000 m. Studies focusing on a transect of elevation gradients show, that changes in microclimate affect the mean flowering time nonlinearly (Rafferty et al., 2020) as well as the flowering synchrony (Fisogni et al., 2022). With our nonlinear approach such studies could be extended across spatio-temporal scales detecting delayed responses across ecological and elevation gradients.

Plant species can develop phenological feedback loops with other species, e.g. the phenology of the tree canopy can affect the phenology of the undergrowth, (Alecrim et al., 2023; Lee et al., 2022; Miller et al., 2023). Crowd-sourced data from mobile applications can provide information on species below the canopy, which is not detectable with satellite remote sensing. In general, our macrophenological approach could examine phenological feedback loops and shifts across a variety of habitats globally.

Climate change affects the seasonal onset, for example spring advancing at rates of 2–7 days per decade (Menzel et al., 2020; Piao et al., 2019). To analyse to what extent seasonal shifts can be detected by our macrophenological approach with crowd-sourced data, multiple years 2020, 2021, 2022 and 2023 could be compared with each other and the average annual cycle. The relationship between MPS, climate variables and photoperiod could be studied, enabling a nuanced understanding of the contribution of climate drivers and the impact of climate change on phenology at macroscales. The extensive versatility of our approach highlights its effectiveness in addressing ecological questions spanning various temporal and spatial scales through individual observations. Yet, achieving this versatility relies heavily on the availability of crowd-sourced data that covers such expansive ranges. Therefore, there is a pressing need for ongoing enhancements and a deeper comprehension of such data to advance our capabilities in exploring macrophenology.

5 | CONCLUSIONS

Our study explores the relationship among simultaneous active phenological states of thousands of species across space and time,

collected via a plant identification app by thousands of citizens. We present a novel macrophenological approach using nonlinear dimension reduction. We showed that the time-varying co-occurrences can be interpreted as a manifestation of phenological group behaviour. We revealed that the macrophenological dynamics are characterised by coherent macroecological patterns during the growing season, which deteriorate during the transition to the non-growing season. This group behaviour, indicating dynamic plant synchronisation, requires further validation from alternative data sources in future research. The crowd-sourced data, obtained via the mobile app for plant classification, Flora Incognita, was essential in our approach. It furnished us with a statistically robust spatio-temporal data set, amassing nearly 10 million observations. We also showed that the entanglement between human data collection behaviour and macrophenological patterns is complex and can be partly mitigated and isolated. Future phenology monitoring should consider the potential of macrophenological approaches based on crowd-sourced data, ideally integrated with other in-situ or remotely sensed observations.

AUTHOR CONTRIBUTIONS

Karin Mora and Miguel D. Mahecha in conversation with Michael Rzanny, Jana Wäldchen, Guido Kraemer, and Patrick Mäder conceived the ideas and designed methodology; Jana Wäldchen, Michael Rzanny and Patrick Mäder prepared the data; Karin Mora analysed the data; Karin Mora wrote the manuscript. All authors discussed and contributed critically to the drafts and gave final approval for publication.

ACKNOWLEDGEMENTS

We thank everyone who shared images and geolocations with Flora Incognita. We thank Ingolf Kühn, Johannes Quaas, and Pedro Leitão for fruitful discussions. We thank Maximilian Söchting for help with improving the presentation of some figures. KM and MDM gratefully acknowledge the support of iDiv funded by the German Research Foundation (DFG–FZT 118, 202548816), iDiv Flexpool project no. 346001237. KM is funded by the Saxon State Ministry for Science, Culture and Tourism (SMWK) (3-7304/35/6-2021/48880). The LU team also acknowledges funding from the DLR for the project ML4Earth. JW, MR, PM acknowledge funding from the German Ministry of Education and Research (BMBF) grant: 01IS20062, the German Federal Ministry for the Environment, Nature Conservation, Building and Nuclear Safety (BMUB) grants: 3519685A08 and 3519685B08, and the Thuringian Ministry for Environment, Energy and Nature Conservation grant: 0901-44-8652. TK acknowledges funding from DFG for the projects PANOPS (grant no. 504978936) and BigPlantSens (grant no. 444524904). DS acknowledges funding from the Volkswagen Foundation (grant-no. 9B937) and Philipp Scshwartz-Initiative of the Alexander von Humboldt-Stiftung (grant no. 232201751). Open Access funding enabled and organized by Projekt DEAL.

CONFLICT OF INTEREST STATEMENT

The authors declare no conflict of interest.

PEER REVIEW

The peer review history for this article is available at https://www.webofscience.com/api/gateway/wos/peer-review/10.1111/2041-210X.14365.

DATA AVAILABILITY STATEMENT

Data and code are publicly available on both platforms Github Digital Repository https://github.com/aperiodik/Macrophenological-dynamics-paper and Zenodo (https://doi.org/10.5281/zenodo.11403407) (Mora et al., 2024).

ORCID

Karin Mora https://orcid.org/0000-0002-3323-4490
Michael Rzanny https://orcid.org/0000-0002-7232-5547
Jana Wäldchen https://orcid.org/0000-0002-2631-1531
Hannes Feilhauer https://orcid.org/0000-0001-5758-6303
Teja Kattenborn https://orcid.org/0000-0001-7381-3828
Guido Kraemer https://orcid.org/0000-0003-4865-5041
Patrick Mäder https://orcid.org/0000-0001-6871-2707
Daria Svidzinska https://orcid.org/0000-0002-1578-6312
Sophie Wolf https://orcid.org/0000-0001-7848-3725
Miguel D. Mahecha https://orcid.org/0000-0003-3031-613X

REFERENCES

Abaid, N., Bollt, E., & Porfiri, M. (2012). Topological analysis of complexity in multiagent systems. *Physical Review E*, *85*, 041907. https://doi.org/10.1103/PhysRevE.85.041907

Alecrim, E. F., Sargent, R. D., & Forrest, J. R. K. (2023). Higher-latitude spring-flowering herbs advance their phenology more than trees with warming temperatures. *Journal of Ecology*, *111*, 156–169. https://doi.org/10.1111/1365-2745.14023

Almeida-Neto, M., & Lewinsohn, T. M. (2004). Small-scale spatial autocorrelation and the interpretation of relationships between phenological parameters. *Journal of Vegetation Science*, *15*, 561–568. https://doi.org/10.1111/j.1654-1103.2004.tb02295.x

Barve, V. V., Brenskelle, L., Li, D., Stucky, B. J., Barve, N. V., Hantak, M. M., McLean, B. S., Paluh, D. J., Oswald, J. A., Belitz, M. W., Folk, R. A., & Guralnick, R. P. (2020). Methods for broad-scale plant phenology assessments using citizen scientists' photographs. *Applications in Plant Sciences*, *8*, e11315. https://doi.org/10.1002/aps3.11315

Binley, A. D., & Bennett, J. R. (2023). The data double standard. *Methods in Ecology and Evolution*, *14*, 1389–1397. https://doi.org/10.1111/2041-210X.14110

Brown, J. H., & Maurer, B. A. (1989). Macroecology: The division of food and space among species on continents. *Science*, *243*, 1145–1150. https://doi.org/10.1126/science.243.4895.1145

Callaghan, C. T., Poore, A. G., Mesaglio, T., Moles, A. T., Nakagawa, S., Roberts, C., Rowley, J. J., VergÉs, A., Wilshire, J. H., & Cornwell, W. K. (2021). Three frontiers for the future of biodiversity research using citizen science data. *BioScience*, *71*, 55–63.

Carl, G., Doktor, D., Koslowsky, D., & Kühn, I. (2013). Phase difference analysis of temperature and vegetation phenology for beech forest: A wavelet approach. *Stochastic Environmental Research and Risk Assessment*, *27*, 1221–1230.

Courter, J. R., Johnson, R. J., Stuyck, C. M., Lang, B. A., & Kaiser, E. W. (2013). Weekend bias in citizen science data reporting: Implications for phenology studies. *International Journal of Biometeorology*, *57*, 715–720.

DeLellis, P., Polverino, G., Ustuner, G., Abaid, N., Macrì, S., Bollt, E. M., & Porfiri, M. (2014). Collective behaviour across animal species. *Scientific Reports*, *4*, 3723.

Doi, H., Gordo, O., Mori, T., & Kubo, M. T. (2017). A macroecological perspective for phenological research under climate change. *Ecological Research*, *32*, 633–641.

Federal Statistical Office. (2011). *2011 census Germany*. https://zensus2011.de/EN/

Fisogni, A., de Manincor, N., Bertelsen, C. D., & Rafferty, N. E. (2022). Long-term changes in flowering synchrony reflect climatic changes across an elevational gradient. *Ecography*, *2022*. https://doi.org/10.1111/ecog.06050

Gajamannage, K., & Bollt, E. M. (2017). Detecting phase transitions in collective behavior using manifold's curvature. *Mathematical Biosciences and Engineering*, *14*, 437–453.

Gajamannage, K., Butail, S., Porfiri, M., & Bollt, E. M. (2015). Identifying manifolds underlying group motion in vicsek agents. *The European Physical Journal Special Topics*, *224*, 3245–3256.

Gallinat, A. S., Ellwood, E. R., Heberling, J. M., Miller-Rushing, A. J., Pearse, W. D., & Primack, R. B. (2021). Macrophenology: Insights into the broad-scale patterns, drivers, and consequences of phenology. *American Journal of Botany*, *108*, 2112–2126. https://doi.org/10.1002/ajb2.1793

Goëau, H., Bonnet, P., Joly, A., Bakić, V., Barbe, J., Yahiaoui, I., Selmi, S., Carré, J., Barthélémy, D., Boujemaa, N., Molino, J.-F., Duché, G., & Péronnet, A. (2013). Pl@ntNet mobile app. In *Proceedings of the 21st ACM international conference on Multimedia* (pp. 423–424). ACM.

Hufkens, K., Melaas, E. K., Mann, M. L., Foster, T., Ceballos, F., Robles, M., & Kramer, B. (2019). Monitoring crop phenology using a smartphone based near-surface remote sensing approach. *Agricultural and Forest Meteorology*, *265*, 327–337.

Jones, H. G. (2020). What plant is that? Tests of automated image recognition apps for plant identification on plants from the british flora. *AoB Plants*, *12*, plaa052.

Katal, N., Rzanny, M., Mäder, P., Römermann, C., Wittich, H. C., Boho, D., Musavi, T., & Wäldchen, J. (2023). Bridging the gap: How to adopt opportunistic plant observations for phenology monitoring. *Frontiers in Plant Science*, *14*, 1150956. https://doi.org/10.3389/fpls.2023.1150956

Katal, N., Rzanny, M., Mäder, P., & Wäldchen, J. (2022). Deep learning in plant phenological research: A systematic literature review. *Frontiers in Plant Science*, *13*, 805738. https://doi.org/10.3389/fpls.2022.805738

Kemppinen, J., Lembrechts, J. J., Van Meerbeek, K., Carnicer, J., Chardon, N. I., Kardol, P., Lenoir, J., Liu, D., Maclean, I., Pergl, J., Saccone, P., Senior, R. A., Shen, T., Słowińska, S., Vandvik, V., von Oppen, J., Aalto, J., Ayalew, B., Bates, O., … De Frenne, P. (2023). Microclimate, an inseparable part of ecology and biogeography. *Zenodo*, https://doi.org/10.5281/zenodo.7973314

Klinger, Y. P., Eckstein, R. L., & Kleinebecker, T. (2023). Iphenology: Using open-access citizen science photos to track phenology at continental scale. *Methods in Ecology and Evolution*, *14*, 1424–1431. https://doi.org/10.1111/2041-210X.14114

Knape, J., Coulson, S. J., van der Wal, R., & Arlt, D. (2022). Temporal trends in opportunistic citizen science reports across multiple taxa. *Ambio*, *51*, 183–198. https://doi.org/10.1007/s13280-021-01550-w

Kraemer, G., Reichstein, M., & Mahecha, M. D. (2018). Dimred and coranking—Unifying dimensionality reduction in r. *R Journal*, *10*, 342–358.

Kühn, I., Bierman, S. M., Durka, W., & Klotz, S. (2006). Relating geographical variation in pollination types to environmental and spatial factors using novel statistical methods. *New Phytologist*, *172*, 127–139. https://doi.org/10.1111/j.1469-8137.2006.01811.x

Kühn, I., Brandl, R., & Klotz, S. (2004). The flora of german cities is naturally species rich. *Evolutionary Ecology Research*, *6*, 749–764.

Lee, B. R., Miller, T. K., Rosche, C., Yang, Y., Heberling, J. M., Kuebbing, S. E., & Primack, R. B. (2022). Wildflower phenological escape differs by continent and spring temperature. *Nature Communications*, *13*, 7157.

Legendre, P., & Legendre, L. (2012). *Numerical ecology* (Vol. *24*). Elsevier. https://www.elsevier.com/books/numerical-ecology/legendre/978-0-444-53868-0

Mäder, P., Boho, D., Rzanny, M., Seeland, M., Wittich, H. C., Deggelmann, A., & Wäldchen, J. (2021). The flora incognita app – Interactive plant species identification. *Methods in Ecology and Evolution*, *12*, 1335–1342. https://doi.org/10.1111/2041-210X.13611

Mahecha, M. D., Martínez, A., Lischeid, G., & Beck, E. (2007). Nonlinear dimensionality reduction: Alternative ordination approaches for extracting and visualizing biodiversity patterns in tropical montane forest vegetation data. *Ecological Informatics*, *2*, 138–149.

Mahecha, M. D., Rzanny, M., Kraemer, G., Mäder, P., Seeland, M., & Wäldchen, J. (2021). Crowd-sourced plant occurrence data provide a reliable description of macroecological gradients. *Ecography*, *44*, 1131–1142. https://doi.org/10.1111/ecog.05492

Mahecha, M. D., & Schmidtlein, S. (2008). Revealing biogeographical patterns by nonlinear ordinations and derived anisotropic spatial filters. *Global Ecology and Biogeography*, *17*, 284–296.

Mainali, K. P., Slud, E., Singer, M. C., & Fagan, W. F. (2022). A better index for analysis of co-occurrence and similarity. *Science Advances*, *8*, eabj9204. https://doi.org/10.1126/sciadv.abj9204

McGill, B. J. (2019). The what, how and why of doing macroecology. *Global Ecology and Biogeography*, *28*, 6–17. https://doi.org/10.1111/geb.12855

Menzel, A., Yuan, Y., Matiu, M., Sparks, T., Scheifinger, H., Gehrig, R., & Estrella, N. (2020). Climate change fingerprints in recent european plant phenology. *Global Change Biology*, *26*, 2599–2612.

Miller, T. K., Heberling, J. M., Kuebbing, S. E., & Primack, R. B. (2023). Warmer temperatures are linked to widespread phenological mismatch among native and non-native forest plants. *Journal of Ecology*, *111*, 356–371. https://doi.org/10.1111/1365-2745.14021

Moles, A. T., & Xirocostas, Z. A. (2022). Statistical power from the people. *Nature Ecology & Evolution*, *6*, 1–2.

Mora, K., Rzanny, M., Wäldchen, J., Feilhauer, H., Kattenborn, T., Kraemer, G., Mäder, P., Svidzinska, D., Wolf, S., & Mahecha, M. D. (2024). *Macrophenological dynamics from citizen science plant occurrence data*. https://github.com/aperiodik/Macrophenological-dynamics-paper

Piao, S., Liu, Q., Chen, A., Janssens, I. A., Fu, Y., Dai, J., Liu, L., Lian, X., Shen, M., & Zhu, X. (2019). Plant phenology and global climate change: Current progresses and challenges. *Global Change Biology*, *25*, 1922–1940. https://doi.org/10.1111/gcb.14619

Primack, R. B., Gallinat, A. S., Ellwood, E. R., Crimmins, T. M., Schwartz, M. D., Staudinger, M. D., & Miller-Rushing, A. J. (2023). Ten best practices for effective phenological research. *International Journal of Biometeorology*, *67*, 1509–1522.

Puchałka, R., Klisz, M., Koniakin, S., Czortek, P., Dylewski, Ł., Paź-Dyderska, S., Vítková, M., Sádlo, J., Rašomavičius, V., Čarni, A., de Sanctis, M., & Dyderski, M. K. (2022). Citizen science helps predictions of climate change impact on flowering phenology: A study on anemone nemorosa. *Agricultural and Forest Meteorology*, *325*, 109133.

Purdy, L. M., Sang, Z., Beaubien, E., & Hamann, A. (2023). Validating remotely sensed land surface phenology with leaf out records from a citizen science network. *International Journal of Applied Earth Observation and Geoinformation*, *116*, 103148.

R Core Team. (2020). *R: A language and environment for statistical computing*. R Foundation for Statistical Computing. https://www.R-project.org/

Rafferty, N. E., Diez, J. M., & Bertelsen, C. D. (2020). Changing climate drives divergent and nonlinear shifts in flowering phenology across elevations. *Current Biology*, *30*, 432–441.

Renner, S. S., & Chmielewski, F.-M. (2021). The International Phenological Garden network (1959 to 2021): Its 131 gardens, cloned study

species, data archiving, and future. *International Journal of Biometeorology*, *66*, 35–43.
Richardson, A. D., Hufkens, K., Milliman, T., Aubrecht, D. M., Chen, M., Gray, J. M., Johnston, M. R., Keenan, T. F., Klosterman, S. T., Kosmala, M., Melaas, E. K., Friedl, M. A., & Frolking, S. (2018). Tracking vegetation phenology across diverse north american biomes using phenocam imagery. *Scientific Data*, *5*, 1–24.
Rzanny, M., Bebber, A., Mäder, P., Wittich, H. C., Boho, D., & Wäldchen, J. (2024). More than rapid identification – free plant identification apps can also be highly accurate. *People and Nature*, in press.
Rzanny, M., Mäder, P., Deggelmann, A., Chen, M., & Wäldchen, J. (2019). Flowers, leaves or both? How to obtain suitable images for automated plant identification. *Plant Methods*, *15*, 1–11.
Rzanny, M., Mäder, P., Wittich, H. C., Boho, D., & Wäldchen, J. (2024). Opportunistic plant observations reveal spatial and temporal gradients in phenology. *npj Biodiversity*, *3*, 5.
Schiller, C., Schmidtlein, S., Boonman, C., Moreno-Martnez, A., & Kattenborn, T. (2021). Deep learning and citizen science enable automated plant trait predictions from photographs. *Scientific Reports*, *11*, 16395.
Sparks, T. H., Huber, K., & Tryjanowski, P. (2008). Something for the weekend? Examining the bias in avian phenological recording. *International Journal of Biometeorology*, *52*, 505–510.
Studer, S., Stöckli, R., Appenzeller, C., & Vidale, P. L. (2007). A comparative study of satellite and ground-based phenology. *International Journal of Biometeorology*, *51*, 405–414.
Tenenbaum, J. B., de Silva, V., & Langford, J. C. (2000). A global geometric framework for nonlinear dimensionality reduction. *Science*, *290*, 2319–2323. https://doi.org/10.1126/science.290.5500.2319
The Global Biodiversity Information Facility. (2023). *What is GBIF? https://gbif.org/what-is-gbif*
Tian, F., Cai, Z., Jin, H., Hufkens, K., Scheifinger, H., Tagesson, T., Smets, B., Van Hoolst, R., Bonte, K., Ivits, E., Ardö, J., & Eklundh, L. (2021). Calibrating vegetation phenology from sentinel-2 using eddy covariance, phenocam, and pep725 networks across europe. *Remote Sensing of Environment*, *260*, 112456.
Unger, S., Rollins, M., Tietz, A., & Dumais, H. (2021). Inaturalist as an engaging tool for identifying organisms in outdoor activities. *Journal of Biological Education*, *55*, 537–547.
van der Maaten, L., Schmidtlein, S., & Mahecha, M. D. (2012). Analyzing floristic inventories with multiple maps. *Ecological Informatics*, *9*, 1–10.
Wagner, F. H. (2021). The flowering of atlantic forest pleroma trees. *Scientific Reports*, *11*, 20437.
Wittich, H. C., Seeland, M., Wäldchen, J., Rzanny, M., & Mäder, P. (2018). Recommending plant taxa for supporting on-site species identification. *BMC Bioinformatics*, *19*, 1–17.
Wohlfahrt, G., Tomelleri, E., & Hammerle, A. (2019). The urban imprint on plant phenology. *Nature Ecology & Evolution*, *3*, 1668–1674.
Wolf, S., Mahecha, M. D., Sabatini, F. M., Wirth, C., Bruelheide, H., Kattge, J., Moreno Martnez, Á., Mora, K., & Kattenborn, T. (2022). Citizen science plant observations encode global trait patterns. *Nature Ecology & Evolution*, *6*, 1–10.
Yuan, Y., Härer, S., Ottenheym, T., Misra, G., Lüpke, A., Estrella, N., & Menzel, A. (2021). Maps, trends, and temperature sensitivities—Phenological information from and for decreasing numbers of volunteer observers. *International Journal of Biometeorology*, *65*, 1377–1390.
Zeng, L., Wardlow, B. D., Xiang, D., Hu, S., & Li, D. (2020). A review of vegetation phenological metrics extraction using time-series, multispectral satellite data. *Remote Sensing of Environment*, *237*, 111511.
Zhang, X., Friedl, M. A., Schaaf, C. B., Strahler, A. H., Hodges, J. C., Gao, F., Reed, B. C., & Huete, A. (2003). Monitoring vegetation phenology using modis. *Remote Sensing of Environment*, *84*, 471–475.

SUPPORTING INFORMATION

Additional supporting information can be found online in the Supporting Information section at the end of this article.

Appendix S1: Data and scaling.

Appendix S2: Macrophenological series: Alternative visualisation.

Appendix S3: Residual variance scaling.

Appendix S4: Scaled residual variance versus counts.

Appendix S5: Isomap computations of aggregated time series with a window length of 45 days.

Appendix S6: Canonical variates of MEPs between consecutive time steps.

Appendix S7: Structural correlations squared.

Appendix S8: Canonical correlations versus observation counts.

How to cite this article: Mora, K., Rzanny, M., Wäldchen, J., Feilhauer, H., Kattenborn, T., Kraemer, G., Mäder, P., Svidzinska, D., Wolf, S., & Mahecha, M. D. (2024). Macrophenological dynamics from citizen science plant occurrence data. *Methods in Ecology and Evolution*, *15*, 1422–1437. https://doi.org/10.1111/2041-210X.14365